Superconducting Circuits for Quantum Simulation of Dynamical Gauge Fields

D. Marcos,[1] P. Rabl,[2] E. Rico,[3] and P. Zoller[1,4]

[1]*Institute for Quantum Optics and Quantum Information of the Austrian Academy of Sciences, A-6020 Innsbruck, Austria*
[2]*Institute of Atomic and Subatomic Physics, TU Wien, Stadionallee 2, 1020 Wien, Austria*
[3]*Institut für Quanteninformationsverarbeitung, Universität Ulm, D-89069 Ulm, Germany*
[4]*Institute for Theoretical Physics, University of Innsbruck, A-6020 Innsbruck, Austria*

(Received 7 June 2013; published 13 September 2013)

We describe a superconducting-circuit lattice design for the implementation and simulation of dynamical lattice gauge theories. We illustrate our proposal by analyzing a one-dimensional U(1) quantum-link model, where superconducting qubits play the role of matter fields on the lattice sites and the gauge fields are represented by two coupled microwave resonators on each link between neighboring sites. A detailed analysis of a minimal experimental protocol for probing the physics related to string breaking effects shows that, despite the presence of decoherence in these systems, distinctive phenomena from condensed-matter and high-energy physics can be visualized with state-of-the-art technology in small superconducting-circuit arrays.

DOI: 10.1103/PhysRevLett.111.110504 PACS numbers: 03.67.Lx, 11.15.Ha, 75.10.Jm, 85.25.−j

The remarkable experimental progress reported in recent years with superconducting quantum circuits (SQCs) has made these systems one of the best platforms for control at the level of single quanta [1–6]. While SQCs have been mainly developed from the perspective of quantum computing, the strong nonlinearities and low loss rates of superconducting devices have inspired proposals and first experimental efforts [7] to implement quantum simulators [8] for spin and Hubbard-type models. Compared to atomic and photonic systems, where many of these concepts were developed first, a key advantage of superconducting devices is that they allow engineering of quantum circuits as basic modules, which can be wired up to design highly nontrivial many-body couplings and dynamics. This makes SQCs a promising platform to simulate lattice models with complex interactions. One of the most interesting and challenging applications along these lines is the implementation of a quantum simulator for lattice gauge theories (LGTs) [9]. It is the purpose of the present work to present designs for SQCs as basic building blocks of LGTs, which can be implemented with existing technology. We illustrate this by analyzing a U(1) lattice model representing quantum electrodynamics (QED) in one dimension (1D), and study dynamical effects related to string breaking in a minimal model of a few coupled lattice sites, which could serve as an example for a first experimental realization.

Gauge theories, and LGTs in particular, play a central role in both particle and condensed-matter physics, and a quantum simulator of such models may provide new insights in regimes not accessible to classical computation. In particle physics, the standard model is formulated as a gauge theory, where interactions between the fundamental constituents of matter are mediated by gauge bosons. Formulation as a LGT [10–12] has enabled a nonperturbative framework, using, for example, Monte Carlo simulations, although most problems concerning finite-density phases and (time-dependent) nonequilibrium dynamics are beyond the scope of these techniques. In condensed-matter physics gauge theories appear in frustrated spin systems and quantum spin liquids [13–16], and a quantum simulator would give access to phases and dynamics thus far out of reach.

In the lattice formulation of gauge theories, the matter fields live on the lattice sites, while the gauge fields appear as bosonic degrees of freedom on the links between neighboring sites [see Fig. 1(a)]. A simple, although nontrivial example of a LGT is the Schwinger model [17–19], representing QED in 1D. This model was analyzed in recent works discussing the implementation of U(1) LGTs with cold atoms [20–29], and can be used as a starting point to illustrate the building blocks for a quantum simulator of gauge theories. To represent the gauge fields, we use the language of quantum-link models (QLMs), which show that the gauge fields can be expressed as spin degrees of freedom [30–32]. The Hamiltonian of the quantum-link version of the Schwinger model is

$$\hat{\mathcal{H}}_{\mathrm{Sch}} = m\sum_{\ell}(-1)^{\ell}\hat{\psi}_{\ell}^{\dagger}\hat{\psi}_{\ell} + g\sum_{\ell}(\hat{S}^{z}_{\ell,\ell+1})^{2} - J\sum_{\ell}(\hat{\psi}_{\ell}^{\dagger}\hat{S}^{+}_{\ell,\ell+1}\hat{\psi}_{\ell+1} + \mathrm{H.c.}). \quad (1)$$

Here, $\hat{\psi}_{\ell}$ is a matter-field operator denoting a (spinless) fermion at lattice site ℓ. The gauge field of this model is represented by the spin operator $\hat{S}$ of a given value $S = 1/2, 1, 3/2, \ldots$, and the z component corresponds to the electric field between lattice sites, $\hat{S}^{z}_{\ell,\ell+1} \equiv \hat{E}_{\ell,\ell+1}$. The simplification introduced by this formulation becomes apparent in the fact that the electric flux can only take discrete values associated with the possible spin states for a given S. The first summand (mass term) in Eq. (1)

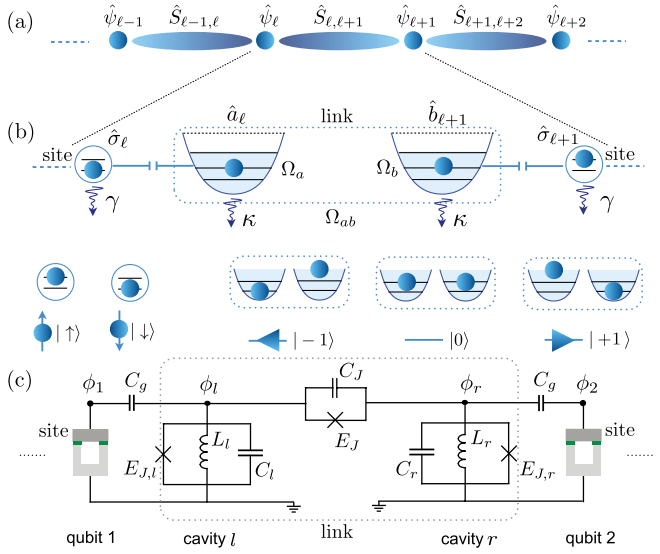

FIG. 1 (color online). (a) Pictorial view of a 1D quantum-link model, where the operators $\hat{\psi}_\ell$ on even (odd) sites represent matter (antimatter) fields and the spin operators $\hat{S}_{\ell,\ell+1}$ residing on each link represent the gauge fields. (b) Equivalent physical implementation, where two-level systems replace the fermionic matter fields and two oscillators with a fixed total number of excitations N encode a spin $S = N/2$ on each link. (c) Superconducting-circuit implementation. Neighboring superconducting qubits on the sites of a 1D lattice are connected via two nonlinear LC resonators.

describes staggered fermions, whose ground state should be interpreted as a filled Dirac sea, and excitations amount to the creation of a particle-antiparticle pair with mass gap m. The second term should be interpreted as an electric-field energy. Finally, the last term (kinetic energy) describes hopping of fermions between two adjacent sites, which is associated with a spin flip $\hat{S}^+_{\ell,\ell+1}$, i.e., a change of the electric field on the link when the charge moves.

The U(1) gauge symmetry is captured as invariance under local transformations of the matter and gauge degrees of freedom, $\hat{V}^\dagger \hat{\psi}_\ell \hat{V} = e^{i\alpha_\ell}\hat{\psi}_\ell$ and $\hat{V}^\dagger \hat{S}^+_{\ell,\ell+1}\hat{V} = e^{i\alpha_\ell}\hat{S}^+_{\ell,\ell+1}e^{-i\alpha_{\ell+1}}$, respectively. The transformation $\hat{V} \equiv \prod_\ell e^{i\alpha_\ell \hat{G}_\ell}$ is generated by $\hat{G}_\ell = \hat{S}^z_\ell - \hat{S}^z_{\ell+1} + \hat{\psi}^\dagger_\ell \hat{\psi}_\ell + [(-1)^\ell - 1]/2$ [33], where $\hat{G}_\ell$ is a conserved quantity, i.e., $[\hat{G}_\ell, \hat{\mathcal{H}}_{\rm Sch}] = 0$. This condition implies that if we initialize our system in an eigenstate of $\hat{G}_\ell$, the dynamics generated by $\hat{\mathcal{H}}_{\rm Sch}$ will remain within the subspace of states $\{|\Psi\rangle\}$ with the same eigenvalue of $\hat{G}_\ell$. In other words (taking for convenience the zero-eigenvalue subspace), gauge invariance implies the constraint $\hat{G}_\ell|\Psi\rangle = 0$. This defines a gauge-invariant set of 'physical' states, and corresponds to the lattice version of the Gauss law $\vec{\nabla}\cdot\vec{E} - \rho = 0$, with $\rho \equiv \hat{\psi}^\dagger_\ell \hat{\psi}_\ell + [(-1)^\ell - 1]/2$.

Superconducting-circuit implementation.—We now describe how to implement the model (1) using a lattice of coupled superconducting circuits. First, we notice that a Jordan-Wigner transformation [34] allows us to express the fermionic fields as two-level systems, $\hat{\psi}_\ell = e^{-i\pi\sum_{m<\ell}(\hat{\sigma}^z_m+1)/2}\hat{\sigma}^z_\ell$ and $\hat{\psi}^\dagger_\ell \hat{\psi}_\ell = (\hat{\sigma}^z_\ell + 1)/2$, where the $\hat{\sigma}^{\pm,z}_\ell$ are Pauli operators, which for our nearest-neighbor coupling does not generate long-range interactions between spins. Second, for each link we consider two resonators with bosonic operators $\hat{a}_\ell$ and $\hat{b}_{\ell+1}$, which encode a general spin $\hat{S}$ through the Schwinger representation $\hat{S}^z_{\ell,\ell+1} \equiv (\hat{a}^\dagger_\ell \hat{a}_\ell - \hat{b}^\dagger_{\ell+1}\hat{b}_{\ell+1})/2$ and $\hat{S}^+_{\ell,\ell+1} \equiv \hat{a}^\dagger_\ell \hat{b}_{\ell+1}$ [35]. In this case, the value of the spin is set by the total number of excitations N per link, $S = N/2$, which can be initially prepared and measured in the experiment [36,37]. The representation of matter and gauge fields in terms of spin and oscillator variables is summarized in Fig. 1(b) for the case $S = 1$. With these new variables the Schwinger model (2) reads

$$\hat{\mathcal{H}}_{\rm Sch} = \frac{m}{2}\sum_\ell (-1)^\ell \hat{\sigma}^z_\ell + \frac{g}{4}\sum_\ell (\hat{a}^\dagger_\ell \hat{a}_\ell - \hat{b}^\dagger_{\ell+1}\hat{b}_{\ell+1})^2 - J\sum_\ell (\hat{\sigma}^+_\ell \hat{a}^\dagger_\ell \hat{b}_{\ell+1}\hat{\sigma}^-_{\ell+1} + \text{H.c.}). \quad (2)$$

As we will show now, this Hamiltonian can be simulated using basic modules of SQCs. To this end, we follow the structure of the building block introduced in Fig. 1(b), where the spins on the lattice sites are simulated with superconducting qubits, while the link between neighboring sites is composed of two coupled nonlinear LC circuits, as shown in Fig. 1(c).

Let us now describe in detail the different circuit components. For the sites we consider conventional superconducting qubits [1–6], which we model by a two-level Hamiltonian $\hat{\mathcal{H}}^{\rm site} = \omega_q \hat{\sigma}_z/2$. Note that the presence of higher, off-resonant qubit levels can slightly modify the effective parameters derived below, but does not qualitatively change the resulting interactions [38]. A link in turn is composed of two coupled LC circuits, each of them in parallel with a Josephson junction to form a nonlinear resonator. This basic element is described by the Hamiltonian $\hat{\mathcal{H}}^{\rm NLC} = \hat{Q}^2/(2C) + \hat{\phi}^2/(2L) - E_J\cos(\hat{\phi}/\phi_0)$ [39–41], where $\hat{\phi}$ and $\hat{Q}$ are canonical flux and charge variables obeying $[\hat{\phi}, \hat{Q}] = i\hbar$, ϕ_0 is the magnetic flux quantum, and E_J the Josephson energy. In the regime, where flux fluctuations are small compared to ϕ_0, the cosine potential can be expanded up to quartic order to obtain $\hat{\mathcal{H}}^{\rm NLC} \approx \omega_a \hat{a}^\dagger\hat{a} - \Omega_a(\hat{a}^\dagger\hat{a})^2$, where $\hat{a}$ and $\hat{a}^\dagger$ are bosonic annihilation and creation operators for electric excitations ("microwave photons") and typically $\omega_a \sim \omega_q \sim$ 5–10 GHz. Ω_a is the strength of the effective Kerr interaction [42–44] and can take values up to several hundred MHz within the validity of the above expansion.

To engineer the interactions of our model with independent coupling constants, the two nonlinear LC resonators

("left" and "right") on each link are coupled via an additional Josephson junction with Josephson energy E_J and a capacitance C_J [cf. Fig. 1(c)]. The total Hamiltonian for a single link is then

$$\hat{\mathcal{H}}^{\text{link}} = \frac{1}{2}\hat{\vec{Q}}\mathcal{C}^{-1}\hat{\vec{Q}}^T + \sum_{\eta=l,r}\frac{\hat{\phi}_\eta^2}{2L_\eta} - \sum_{\eta=l,r}E_{J,\eta}\cos\left(\frac{\hat{\phi}_\ell}{\phi_0}\right) - E_J\cos\left(\frac{\hat{\phi}_l-\hat{\phi}_r}{\phi_0}\right), \quad (3)$$

where $\hat{\vec{Q}} \equiv (\hat{Q}_l, \hat{Q}_r)$, $\mathcal{C}$ is the capacitance matrix [38], and $E_{J,\eta}$ and L_η denote Josephson energies and inductances as shown in Fig. 1(c). As above, we expand the Josephson terms up to quartic order and by keeping only near-resonant terms we obtain a Hamiltonian of the form [38,45–47]

$$\hat{\mathcal{H}}^{\text{link}} = \omega_a\hat{a}^\dagger\hat{a} + \omega_b\hat{b}^\dagger\hat{b} - \Omega_a(\hat{a}^\dagger\hat{a})^2 - \Omega_b(\hat{b}^\dagger\hat{b})^2 - \Omega_{ab}\hat{a}^\dagger\hat{a}\hat{b}^\dagger\hat{b} + \hat{\mathcal{H}}^{\text{nc}}. \quad (4)$$

Here $\hat{a}$ and $\hat{b}$ are bosonic operators for quasilocalized excitations of the left and right resonators, respectively, and ω_a and ω_b are the corresponding mode frequencies. Ω_a, Ω_b, and Ω_{ab} denote the strengths of self- and cross-Kerr nonlinearities. Finally, $\hat{\mathcal{H}}^{\text{nc}}$ accounts for additional, gauge-variant interactions of the form $\sim\hat{a}^\dagger\hat{a}^\dagger\hat{b}\,\hat{b}$, $\sim\hat{a}^\dagger\hat{a}\,\hat{a}\,\hat{b}$ [38]. To suppress photon processes induced by $\hat{\mathcal{H}}^{\text{nc}}$, we will consider the conditions $\Omega_a \approx \Omega_b \approx \Omega_{ab}/2$, and $|\omega_a - \omega_b| \gg \Omega_a, \Omega_b, \Omega_{ab}$. A more detailed discussion and a specific example showing how this can be done is presented in [38].

Finally, the coupling between sites and adjacent links is realized by a small capacitance C_g, which for near-resonant subsystems results in a Jaynes-Cummings coupling $\hat{\mathcal{H}}_\ell^\lambda = \lambda\hat{\sigma}_\ell^\dagger(\hat{a}_\ell + \hat{b}_\ell) + \text{H.c.}$ Altogether, the Hamiltonian of the full circuit lattice takes the form $\hat{\mathcal{H}}_{\text{micro}} = \sum_\ell \hat{\mathcal{H}}_\ell^{\text{site}} + \hat{\mathcal{H}}_{\ell,\ell+1}^{\text{link}} + \hat{\mathcal{H}}_\ell^\lambda$, and written in a rotating frame reads

$$\hat{\mathcal{H}}_{\text{micro}} \approx \frac{\Delta}{2}\sum_\ell(-1)^\ell\hat{\sigma}_\ell^z + \frac{g}{4}\sum_\ell(\hat{a}_\ell^\dagger\hat{a}_\ell - \hat{b}_{\ell+1}^\dagger\hat{b}_{\ell+1})^2 + \delta\sum_\ell\hat{N}_\ell - W\sum_\ell\hat{N}_\ell^2 + \sum_\ell\hat{\mathcal{H}}_\ell^\lambda. \quad (5)$$

Here we have regrouped the nonlinearities in Eq. (4) in terms of the total photon number per link, $\hat{N}_\ell \equiv \hat{a}_\ell^\dagger\hat{a}_\ell + \hat{b}_{\ell+1}^\dagger\hat{b}_{\ell+1}$, and the difference $\hat{S}_{\ell,\ell+1}^z \equiv (\hat{a}_\ell^\dagger\hat{a}_\ell - \hat{b}_{\ell+1}^\dagger\hat{b}_{\ell+1})/2$, representing the discrete electric-field variable. The corresponding interaction scales are given by $W \equiv (\Omega_a + \Omega_b + \Omega_{ab})/4$ and $g \equiv \Omega_{ab} - \Omega_a - \Omega_b$, and Δ and δ denote qubit and resonator detunings from a common frequency offset, respectively.

By identifying $m \equiv \Delta$ the first line of Eq. (5) already reproduces the mass term and the electric-field energy of the QLM (1). To realize the gauge-invariant tunneling term $\sim J$, we consider $W \gg \lambda, g$, which restricts our model to a subset of states with well-defined photon number per link, $\hat{N}_\ell|\psi\rangle = N_0|\psi\rangle$, since the addition or subtraction of a photon is suppressed by an energy penalty $\Delta E_\pm \equiv \mp(\delta - 2N_0W) - W$. Furthermore, this allows us to treat $\hat{\mathcal{H}}_\ell^\lambda$ perturbatively, which to second order gives the coupling $-J\sum_\ell(\hat{\sigma}_\ell^+\hat{a}_\ell\hat{b}_{\ell+1}^\dagger\hat{\sigma}_\ell^- + \text{H.c.})$, with $J = -\lambda^2(1/\Delta E_+ + 1/\Delta E_-)$. By choosing an optimal detuning $\delta = 2N_0W$ and undoing the substitutions given by the Schwinger and Jordan-Wigner mappings, we obtain Eq. (1), with effective parameters $m \equiv \Delta$, $J \approx -2\lambda^2/W$, and g defined above. For realistic values $W/(2\pi) \approx 200$ MHz and $\lambda/(2\pi) \approx 30$ MHz, the resulting energy scales of our model J, g, m are around a few MHz, which are considerably larger than the typical decoherence rates $\sim$10 kHz obtained with state-of-the-art superconducting devices [48,49].

String breaking.—To illustrate, how the physics associated with the model of Eq. (2) can be probed in experiments, here we focus on phenomena related to string breaking [50–52]. This effect is of particular interest in quantum chromodynamics, and by adopting the terminology from this field, its counterpart in the present 1D model can be intuitively understood as follows. Starting from the "vacuum" state with $\langle\hat{S}_{\ell,\ell+1}^z\rangle = 0$, $\langle\hat{\sigma}_\ell^z\rangle = (-1)^{\ell+1}$, and energy E_0, a "quark-antiquark" pair can be created by flipping the spin of two neighboring sites and—to conserve the Gauss law—adding a flux $\langle\hat{S}_{\ell,\ell+1}^z\rangle = \pm 1$ on the link between them. Assuming $J \ll m$, this state has an energy $E_0 + 2m + g$. By increasing the separation between the matter-antimatter excitation and adding the corresponding fluxes on each link, the energy of the resulting "string," $E_{\text{string}} = E_0 + 2m + g(L-1)$, increases linearly with the number of lattice sites L from quark to antiquark. Eventually, when $L \geq 2m/g + 3$, it becomes energetically more favorable to break the string and use the available electric-field energy to create two additional particles, forming two disconnected "mesons" (quark-antiquark pairs with corresponding flux lines), with a total energy $E_{\text{meson}} = E_0 + 4m + 2g$.

Figure 2(a) shows the spin configurations corresponding to meson and string states, given a minimal setting with $L = 4$ sites. Since the matter and antimatter excitations at the two ends of the chain represent the fixed quark-antiquark configuration, the dynamics in this case involves only a single unit cell consisting of two qubits and a single link [as realized by the circuit shown in Fig. 1(c)]. In terms of Schwinger bosons, the states correspond to $|\text{meson}\rangle = |\uparrow; n_a = 1, n_b = 1; \downarrow\rangle$ and $|\text{string}\rangle = |\downarrow; n_a = 2, n_b = 0; \uparrow\rangle$. In Fig. 2(b) we plot the relevant energy levels of the effective model (1) as a function of the (tunable) mass m. For the parameter regime considered above, we find a qualitatively good agreement with the energies obtained directly from the underlying microscopic model (5). For $m/g \ll -1$, the

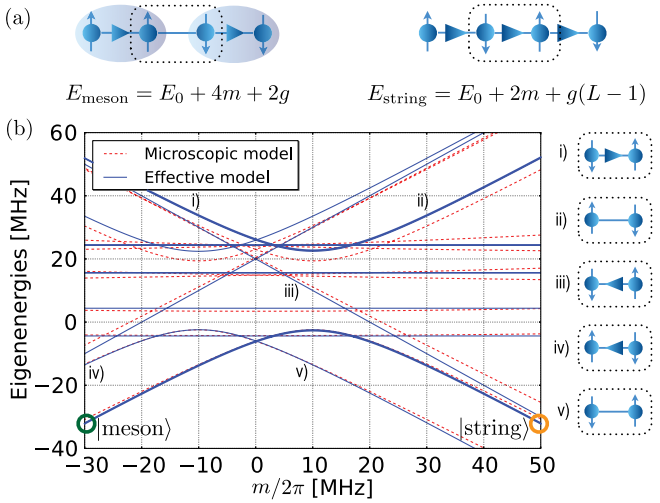

FIG. 2 (color online). (a) Schematic representation of the states $|\text{meson}\rangle$ (left) and $|\text{string}\rangle$ (right) for a lattice of $L = 4$ sites. The spins (matter-antimatter excitations) at the end of the chain are considered fixed and the gauge-invariant dynamics in this minimal setting only involves a single unit cell with two sites and one link as indicated by the dashed box. (b) Spectrum of the microscopic Hamiltonian [Eq. (5)] and effective model [Eq. (1)] for a single unit cell. The thick solid lines show the energies of the states $|\text{meson}\rangle$ and $|\text{string}\rangle$, which transform into each other via an avoided crossing (symmetric and antisymmetric superpositions of these states) at $m \approx g/2$. Other lines correspond to spin combinations that for the boundary conditions defined in (a) are not consistent with the Gauss law $\hat{G}_\ell|\psi\rangle = 0$. The parameters for this plot are $\Omega_a = \Omega_b = 2\pi \times 200$ MHz. $\Omega_{ab} = 2\pi \times 420$ MHz, $\lambda = 2\pi \times 30$ MHz, $W = (\Omega_a + \Omega_b + \Omega_{ab})/4 = 2\pi \times 205$ MHz. The energy splitting is given by $2\sqrt{2}J$, and the effective parameters are $|J| \approx 2\lambda^2/W = 2\pi \times 8.78$ MHz and $g = \Omega_{ab} - \Omega_a - \Omega_b = 2\pi \times 20$ MHz.

state $|\text{meson}\rangle$ is an approximate eigenstate of the Hamiltonian, which in an actual experiment can be prepared by exciting the first qubit and initializing each resonator with a single photon. As we increase m, the meson and string states are hybridized, giving for $m \approx g/2$ an anticrossing split by $2\sqrt{2}J$, and finally an eigenstate $|\text{string}\rangle$ for $m/g \gg 1$.

To study the feasibility of the proposal under realistic conditions, we include the effect of a Markovian cavity and qubit decay, and model the system dynamics by a master equation:

$$\frac{d}{dt}\hat{\rho} = -i[\hat{\mathcal{H}}, \hat{\rho}] + \frac{\gamma}{2}\sum_\ell (2\hat{\sigma}_\ell^- \hat{\rho}\hat{\sigma}_\ell^+ - \{\hat{\sigma}_\ell^+\hat{\sigma}_\ell^-, \hat{\rho}\}) + \kappa\sum_\ell (2\hat{a}_\ell\hat{\rho}\hat{a}_\ell^\dagger - \{\hat{a}_\ell^\dagger\hat{a}_\ell, \hat{\rho}\} + 2\hat{b}_\ell\hat{\rho}\hat{b}_\ell^\dagger - \{\hat{b}_\ell^\dagger\hat{b}_\ell, \hat{\rho}\}). \tag{6}$$

Here, $\hat{\rho}$ is the density operator, γ and κ are qubit and resonator relaxation rates, respectively, and for $\hat{\mathcal{H}}$ we use the microscopic model given in Eq. (5).

In Fig. 3 we show the results from a numerical simulation of the experiment described above, where the state $|\text{meson}\rangle$ is initially prepared and converted into the state $|\text{string}\rangle$ by an adiabatic Landau-Zener sweep through the avoided crossing. In Fig. 3(a) we have calculated the fidelity $\langle\Psi_f|\hat{\rho}|\Psi_f\rangle$ of finding the state $|\Psi_f\rangle \approx |\text{string}\rangle$, starting from $|\Psi_i\rangle \approx |\text{meson}\rangle$, and performing a detuning sweep of the form $m(t) = m_i + vt$ between $m = m_i = -2\pi \times 30$ MHz and $m = m_f = 2\pi \times 50$ MHz. In the absence of dissipation the meson-to-string transition probability follows the standard Landau-Zener formula $P_{m\to s} = 1 - \exp(-2\pi J^2/v)$, and the fidelity decreases monotonically as a function of the sweep velocity v. This imposes a minimal experimental time scale $T \equiv (m_f - m_i/v) \gg J^{-1}$ to observe the transition. In the presence of losses, an upper bound is set by κT, $\gamma T \ll 1$, to avoid the decay out of the initially prepared subspace. Figure 3(a) shows that for realistic loss rates a suitable intermediate time scale, corresponding to a sweep velocity $v_{\text{opt}}/(2\pi) \approx 2\pi \times 100$ MHz/μs, with transfer fidelities

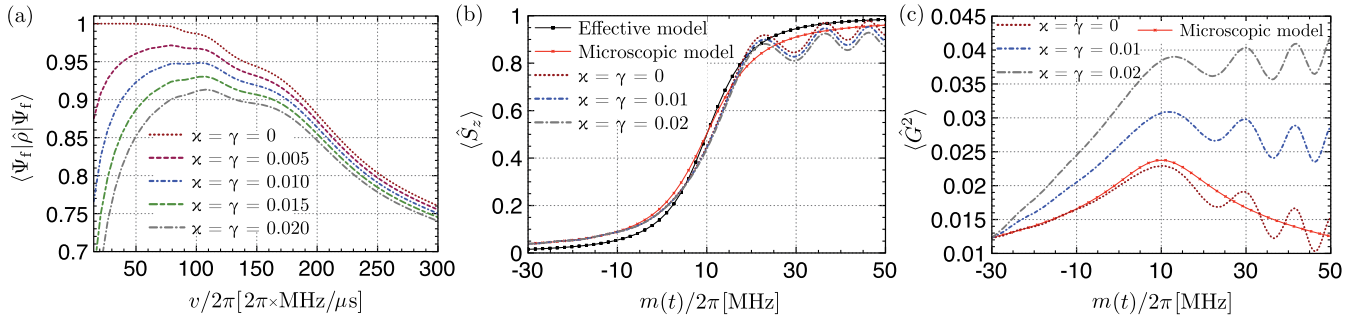

FIG. 3 (color online). Parameters as in Fig. 2(c) and values in the legends in $2\pi \times$ MHz. (a) Fidelity of the state $|\Psi_f\rangle \approx |\text{string}\rangle$ [eigenstate at $m/(2\pi) = 50$ MHz] after a Landau-Zener sweep from the state $|\Psi_i\rangle \approx |\text{meson}\rangle$ [eigenstate at $m/(2\pi) = -30$ MHz]. m is changed proportionally to a constant speed v. (b) Meson-string transition, shown by the average value of the spin on the link, choosing $v/(2\pi) = 2\pi \times 100$ MHz/μs and starting from the state $|\Psi_i\rangle \approx |\text{meson}\rangle$. The result from a Landau-Zener sweep compares well with the static case of the microscopic and effective models (solid lines). Oscillations are present in the string phase due to the nonadiabaticity of the sweep. (c) Gauss-law violation through the sweep, choosing $v/(2\pi) = 2\pi \times 100$ MHz/μs, which compares well with the static case (solid line). The effective model has, by construction, $\langle\hat{G}^2\rangle = 0$.

~95% can be identified. Choosing this sweep velocity, we study the onset of the meson-string transition by monitoring the magnetization $\langle \hat{S}_z \rangle$ at the middle link. This is shown in Fig. 3(b), where, as predicted, we observe a crossover from $\langle \hat{S}_z \rangle = 0$ to $\langle \hat{S}_z \rangle = 1$. Oscillations seen in the string region are due to nonadiabatic effects arising from a finite ramping time [53]. For current experimental parameters, the transition can be clearly observed and compares well with both the behavior predicted by the effective model (1) and the microscopic Hamiltonian (5). In Fig. 3(c) we plot the expectation value $\langle \hat{G}^2 \rangle$, which quantifies the violation of the Gauss law $\hat{G}|\Psi\rangle = 0$ across the transition. This violation comes from the gauge-variant term $\hat{\mathcal{H}}^{\lambda}$ present in the microscopic Hamiltonian as well as the decay out of the initial subspace given by the Lindblad terms in Eq. (6). Starting from a finite value $\langle \hat{G}^2 \rangle \approx 1\%$ determined by $\hat{\mathcal{H}}^{\lambda}_{\ell}$ in the microscopic Hamiltonian, $\langle \hat{G}^2 \rangle$ reaches a local maximum at the anticrossing. For larger decay rates the violation of the Gauss law eventually increases linearly with time due to losses. However, the overall violation remains sufficiently small for state-of-the-art decoherence rates and required experimental ramping times.

Scalability.—The analysis presented above shows that nontrivial phenomena, such us dynamics related to string breaking, can already be observed within a single unit cell composed of two sites and one link. Using this building block, the simulation of this and other dynamical phenomena can be successively scaled up to larger lattices. For the example of string breaking, the string and the meson states can be distinguished by measuring the average magnetization $M \equiv (1/S(L-1))\sum_{\ell} S^z_{\ell,\ell+1}$, which ideally varies sharply from 0 to 1 across the transition and is also robust with respect to individual decay processes. Note that, while for larger systems the total loss rate increases as $\Gamma_L = \gamma L + 4\kappa(L-1)$, a decay out of the physical subspace can be detected by measuring the qubit and photon populations at the end of the experiment. Therefore, for moderate system sizes and experimental time scales $T \sim \Gamma_L^{-1}$, accurate quantum simulations can still be performed by looking at postselected results [54]. By further increasing the system size, the meson-string transition eventually becomes nonadiabatic. In this case we expect a string fragmentation [52] with competing length scales determined by the Kibble-Zurek mechanism and the occurrence of random defects due to photon loss, respectively. The role of dissipation in LGTs is by itself a challenging and largely unexplored problem, which in the present context can be addressed by adjusting the coherent and dissipative time scales in a controlled manner.

Conclusions and outlook.—In summary, we have described the implementation of the essential building blocks of a superconducting quantum simulator for dynamical lattice gauge field theories, where the basic physical effects can already be analyzed with an experimentally available number of coupled superconducting circuits [55]. The extension of this work to two-dimensional [56] and non-Abelian interactions may eventually allow us to use such superconducting architecture for addressing open problems present in condensed-matter and high-energy physics.

We thank R. Schoelkopf, U.-J. Wiese, M. Hafezi, M. Dalmonte, G. Kirchmair, M. Mariantoni, M. Büttiker, F. Sols, and J. Majer for stimulating discussions. This work was supported by the EU project SIQS and the Austrian Science Fund (FWF) through SFB FOQUS and the START Grant No. Y 591-N16.

[1] Y. Makhlin, G. Schön, and A. Shnirman, Rev. Mod. Phys. **73**, 357 (2001).
[2] M. H. Devoret and J. M. Martinis, Quantum Inf. Process. **3**, 163 (2004).
[3] R. J. Schoelkopf and S. M. Girvin, Nature (London) **451**, 664 (2008).
[4] J. Clarke and F. K. Wilhelm, Nature (London) **453**, 1031 (2008).
[5] J. Q. You and F. Nori, Nature (London) **474**, 589 (2011).
[6] M. H. Devoret and R. J. Schoelkopf, Science **339**, 1169 (2013).
[7] D. L. Underwood, W. E. Shanks, J. Koch, and A. A. Houck, Phys. Rev. A **86**, 023837 (2012).
[8] A. A. Houck, H. E. Türeci, and J. Koch, Nat. Phys. **8**, 292 (2012).
[9] U.-J. Wiese, Ann. Phys. (Berlin), doi:10.1002/andp.201300104 (2013).
[10] K. G. Wilson, Phys. Rev. D **10**, 2445 (1974).
[11] J. Kogut and L. Susskind, Phys. Rev. D **11**, 395 (1975).
[12] C. Gattringer and C. B. Lang, *Quantum Chromodynamics on the Lattice* (Springer-Verlag, Berlin, 2010).
[13] J. B. Kogut, Rev. Mod. Phys. **51**, 659 (1979).
[14] X.-G. Wen, *Quantum Field Theory of Many-body Systems* (Oxford University Press, New York, 2004).
[15] C. Lacroix, P. Mendels, and F. Mila, *Introduction to Frustrated Magnetism* (Springer-Verlag, Berlin, 2011).
[16] L. Balents, Nature (London) **464**, 199 (2010).
[17] J. Schwinger, Phys. Rev. **128**, 2425 (1962).
[18] T. Banks, L. Susskind, and J. Kogut, Phys. Rev. D **13**, 1043 (1976).
[19] S. Coleman, Ann. Phys. (N.Y.) **101**, 239 (1976).
[20] E. Kapit and E. Mueller, Phys. Rev. A **83**, 033625 (2011).
[21] E. Zohar and B. Reznik, Phys. Rev. Lett. **107**, 275301 (2011).
[22] D. Banerjee, M. Dalmonte, M. Müller, E. Rico, P. Stebler, U.-J. Wiese, and P. Zoller, Phys. Rev. Lett. **109**, 175302 (2012).
[23] E. Zohar, J. I. Cirac, and B. Reznik, Phys. Rev. Lett. **109**, 125302 (2012).
[24] E. Zohar, J. I. Cirac, and B. Reznik, Phys. Rev. Lett. **110**, 055302 (2013).
[25] L. Tagliacozzo, A. Celi, A. Zamora, and M. Lewenstein, Ann. Phys. (Amsterdam) **330**, 160 (2013).
[26] D. Banerjee, M. Bögli, M. Dalmonte, E. Rico, P. Stebler, U.-J. Wiese, and P. Zoller, Phys. Rev. Lett. **110**, 125303 (2013).

[27] E. Zohar, J. I. Cirac, and B. Reznik, Phys. Rev. Lett. **110**, 125304 (2013).
[28] L. Tagliacozzo *et al.*, arXiv:1211.2704.
[29] E. Zohar, J. I. Cirac, and B. Reznik, Phys. Rev. A **88**, 023617 (2013).
[30] D. Horn, Phys. Lett. **100B**, 149 (1981).
[31] P. Orland and D. Rohrlich, Nucl. Phys. **B338**, 647 (1990).
[32] S. Chandrasekharan and U.-J Wiese, Nucl. Phys. **B492**, 455 (1997).
[33] The last term in the generators has been included due to the staggered-fermion configuration.
[34] P. Jordan and E. Wigner, Z. Phys. **47**, 631 (1928).
[35] A. Auerbach, *Interacting Electrons and Quantum Magnetism* (Springer-Verlag, New York, 1994).
[36] M. Hofheinz *et al.*, Nature (London) **459**, 546 (2009).
[37] D. Bozyigit *et al.*, Nat. Phys. **7**, 154 (2011).
[38] See Supplemental Material at http://link.aps.org/supplemental/10.1103/PhysRevLett.111.110504 for details on the quantum-link model with superconducting circuits.
[39] M. H. Devoret, in *Quantum Fluctuations*, edited by S. Reynaud, E. Giacobino, and J. Zinn-Justin (Elsevier, Amsterdam, 1997), pp. 351–385.
[40] J. Koch, T. M. Yu, J. Gambetta, A. A. Houck, D. I. Schuster, J. Majer, A. Blais, M. H. Devoret, S. M. Girvin, and R. J. Schoelkopf, Phys. Rev. A **76**, 042319 (2007).
[41] V. E. Manucharyan, J. Koch, L. I. Glazman, and M. H. Devoret, Science **326**, 113 (2009).
[42] J. A. Schreier, A. A. Houck, J. Koch, D. I. Schuster, B. R. Johnson, J. M. Chow, J. M. Gambetta, J. Majer, L. Frunzio, M. H. Devoret, S. M. Girvin, and R. J. Schoelkopf, Phys. Rev. B **77**, 180502 (2008).
[43] F. R. Ong, M. Boissonneault, F. Mallet, A. C. Doherty, A. Blais, D. Vion, D. Esteve, and P. Bertet, Phys. Rev. Lett. **110**, 047001 (2013).
[44] G. Kirchmair, B. Vlastakis, Z. Leghtas, S. E. Nigg, H. Paik, E. Ginossar, M. Mirrahimi, L. Frunzio, S. M. Girvin, and R. J. Schoelkopf, Nature (London) **495**, 205 (2013).
[45] A. V. Sharypov, X. Deng, and L. Tian, Phys. Rev. B **86**, 014516 (2012).
[46] S. E. Nigg, H. Paik, B. Vlastakis, G. Kirchmair, S. Shankar, L. Frunzio, M. H. Devoret, R. J. Schoelkopf, and S. M. Girvin, Phys. Rev. Lett. **108**, 240502 (2012).
[47] J. Jin, D. Rossini, R. Fazio, M. Leib, and M. J. Hartmann, Phys. Rev. Lett. **110**, 163605 (2013).
[48] H. Paik *et al.*, Phys. Rev. Lett. **107**, 240501 (2011).
[49] R. Barends *et al.*, Phys. Rev. Lett. **111**, 080502 (2013).
[50] J. Potvin, Phys. Rev. D **32**, 2070 (1985).
[51] M. Pepe and U.-J. Wiese, Phys. Rev. Lett. **102**, 191601 (2009).
[52] F. Hebenstreit, J. Berges, and D. Gelfand, arXiv:1307.4619.
[53] See K. Kim *et al.*, New J. Phys. **13**, 105003 (2011); R. Islam *et al.*, Nat. Commun. **2**, 377 (2011) for a discussion of the same effect in the context of the Ising transition with trapped ions.
[54] T. Fukuhara *et al.*, Nat. Phys. **9**, 235 (2013).
[55] E. Lucero *et al.*, Nat. Phys. **8**, 719 (2012).
[56] D. Marcos *et al.* (unpublished).